Poly(L-lysine)/Microcrystalline Cellulose Biocomposites for Porous Scaffolds

Mohamed Eldessouki, Gisela Buschle-Diller, Yasser Gowayed
Department of Polymer and Fiber Engineering, Auburn University, Alabama 36849-5327

The need for tissue engineered scaffolds is growing due to a shortage in organ donation, potential immunoreactions to allotransplants, and high cost associated with transplantation. The main focus of this research is concerned with material selection and processing which are key for a successful design of any tissue engineered structure. This work investigates the possibility of reinforcing a weak polypeptide [poly(L-lysine)] with a stronger polysaccharide (cellulose) and processing the resulting composite into a porous structure. As the main processing parameters, the effect of pH on the secondary structure of the polypeptide and the effect of the hydrolysis conditions on the properties of commercially available microcrystalline cellulose (MCC) were studied. The significance of the cellulose content as well as the scaffold fabrication conditions on the properties of the composite system was assessed. Overall, PLL/MCC composites showed a lower crystallinity compared to the PLL alone while further hydrolyzed MCC particles (HMCC) showed surface erosion and resulted in a crystallinity increase when incorporated into a composite structure. POLYM. COMPOS., 32:1937–1944, 2011. © 2011 Society of Plastics Engineers

INTRODUCTION

Scaffold formation is one of the key elements for regenerative medicine where a bioresorbable material is implanted in the body to form a three-dimensional template for cell adhesion [1]. Scaffolds also provide the temporary mechanical support needed during cell growth [2]. The ideal scaffold material should have the following characteristics [3, 4]: (a) high surface area with interconnected pores to allow cell growth and the flow transport of nutrients and metabolic waste; (b) biocompatibility and bioresorbability with controlled rates of degradation and resorption to match cell and tissue growth; (c) proper surface chemistry for cell attachment, proliferation, and differentiation, and (d) mechanical properties to match those of the tissue at the site of implantation.

Correspondence to: Yasser Gowayed; e-mail: gowayya@auburn.edu
DOI 10.1002/pc.21220
Published online in Wiley Online Library (wileyonlinelibrary.com).

A promising candidate for a scaffold material is poly(L-lysine), (PLL). PLL is a biocompatible polymer with its lysine repeat units being essential building blocks of proteins in mammals. It is bioresorbable and produces acetyl-coenzyme A during metabolization, a process important for many of the body's biochemical reactions [5]. The bulk properties of PLL are affected by the secondary structure of its chains that take different conformations (α-helix, β-platelet sheets, or random coils) depending on the micro-environment (e.g., temperature and pH) of the molecules [6, 7] and their molecular weight [8]. In each specific secondary structure, the accessible functional groups determine potential sites for interaction with proteins that assist cell adhesion and growth [9, 10]. Therefore, PLL could be referred to as a "smart" polymer since it is able to change its properties according to the surrounding conditions and additionally by stimulants such as incident light [11].

As a polycation under biological conditions [12], PLL can support the attachment of negatively charged cells of the body to its surface [13, 14] which makes it a good choice as a scaffold material [15, 16]. Its cationic surface charge has been utilized in numerous medical applications where self-assembling is decisive [17] as well as for coating applications of other biomaterials [14]. It allows the development of electrostatic interactions between the primary amines of the polymer and the phosphates in DNA [10]. For example, the amount of immobilized DNA was found to increase after coating membranes of poly(2-hydroxyethyl methacrylate), (pHEMA) with a layer of PLL [14]. The membranes were utilized for therapy of autoimmune diseases involving the removal of anti-DNA antibodies from plasma and led to significant improvements [18]. PLL is a widely studied polycation for alginate bead coating used to stabilize and control the molecular weight cut-off of microcapsule membranes [19]. The modification of the surface of these microcapsules showed to be advantageous to overcoming the immunogenic effect of PLL at certain concentrations [20, 21]. PLL was copolymerized with other biopolymers, such as poly(lactic acid) (PLA) to form a biomaterial that can impact cell behavior *in vitro* [22]. For selective cell adhesion, PLL blends and copolymers were modified through the

derivatization of arginine-glycine-aspartic acid (RGD) motifs which are ligands for integrin cell adhesion receptors [23].

Although PLL has potential advantages for tissue engineering materials, its application has been limited to surface property enhancements of scaffolds made from other polymers [24, 25]. This limitation is due to its relatively weak structure and its hydrophilicity. Attempts have been carried out to counteract its poor mechanical properties by reinforcing PLL with nanoclays [7], carbon nanotubes [26], and bioceramic particles of hydroxyapatite [27].

Systems of polypeptides with cellulose were described in literature [28] where different proteins, including PLL, were used as thin laminating layers for cellulosic paper films to enhance their wet strength because the fibers showed swelling and loss of adhesive contact. The optimum wet strength was achieved in samples with highest contents of lysine and arginine, and for samples that were processed at elevated temperature which provided an opportunity for covalent bond formation between cellulose and peptide. The biocompatibility of cellulose is well-known and microcrystalline cellulose (MCC) particles are inherently fairly stiff and could act as reinforcement for the PLL matrix. A hypothetically perfect crystalline phase of MCC has an estimated modulus of ~150 GPa [29].

This research focuses on the possibility of reducing the hydrophilicity of PLL and creating a tissue engineered scaffold with reasonable swelling capabilities by incorporating MCC particles. Although osteoconductive, cellulose by itself does not stimulate cell growth and would need a compound such as PLL to synergistically recruit cells while keeping the scaffold sufficiently stable. The presented work mainly focuses on the effect of processing conditions on both MCC and PLL as the crystallinity level of the MCC is changed through hydrolysis, and by altering the pH of the PLL solution. The MCC content was also varied to study its correlation with the properties of the scaffold.

There is a variety of methods to fabricate scaffolds such as salt leaching, membrane lamination, super critical-fluid foaming, solid free form fabrication, and thermally induced phase separation (TIPS) [3]. Each of these methods has its own advantages and limitations, in regard to the resulting geometry of the pores, the pore structure or the overall homogeneity of the scaffold [30, 31]. For this work, TIPS was employed and the impact of the freezing temperature on the scaffold porosity and pore size distribution was evaluated.

EXPERIMENTAL WORK

Materials

Microcrystalline cellulose (MCC) and poly(L-lysine-hydrobromide), (PLL) were purchased from Sigma–Aldrich. The chemical structure of PLL is shown in Fig. 1 and has an average molecular weight of 150 kD as provided by the supplier. All other chemicals were obtained from Fisher Chemicals.

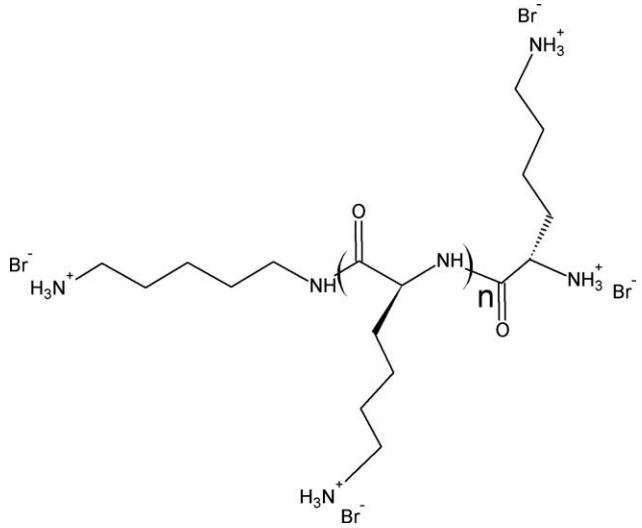

FIG. 1. Chemical structure of poly(L-lysine-hydrobromide).

Sample Preparation

Samples were prepared at pH 7 and 11.6 by dissolving a 100 mg PLL in 250 mL 0.1 M buffer solution with overnight stirring followed by sonication for 5 min in a bath sonicator, Branson 3510. The samples were casted on a Teflon® plate and dried in an oven at 60°C for 48 h to produce a film. The buffer solutions were prepared using a 0.1 M solution of monobasic potassium phosphate (KH_2PO_4) titrated to pH 7 and pH 11.6, respectively, with a 0.1 M potassium hydroxide (KOH) solution.

Cellulose Hydrolysis

Microcrystalline cellulose (MCC) was dispersed in a 50% sulfuric acid at a ratio of MCC:H_2SO_4 1:8.75 [32]. The dispersion was equilibrated in an oil bath at 45°C with vigorous stirring for 2 h. One set of samples (HMCC) was sonicated using a tip sonicator for 5 min at 30% amplitude with 30-s intervals and 5 s pausing; a second set (HMCC-NS) was directly washed without sonication. During sonication, a thermostated water bath was used to avoid the removal of sulfate groups on the surface of MCC by accidental overheating [33]. After sonication the sample was centrifuged at 6,700 rpm for 10 min and washed repeatedly with deionized water until the pH of the solution became 5.

PLL/MCC and HMCC Composite Preparation

MCC and HMCC particles were dispersed in 25 ml of deionized water (pH 7) at various concentrations (see Table 1). The dispersion was placed in a bath sonicator for 20 min with a bath temperature of 25°C. Measured

 DOI 10.1002/pc

TABLE 1. Sample designation.

Sample designation	MCC (%)	HMCC (%)	Preparation
PLC00	0	0	Dissolved in water (pH 7)
PLC02	2	0	Dissolved in water (pH 7)
PLC05	5	0	Dissolved in water (pH 7)
PLC10	10	0	Dissolved in water (pH 7)
PLC15	15	0	Dissolved in water (pH 7)
PLHC05	0	5	Sonication during hydrolysis
PLHC05-NS	0	5	No sonication during hydrolysis

amounts of PLL were added to each container, and then sonicated for 30 min at the same temperature. The sonicator was turned to the degas mode for 10 min to remove air bubbles from the solution.

Scaffold Fabrication

The composite solutions prepared in the previous step were prefrozen at temperatures of -23°C for 3 h to solidify at a cooling rate of 1°C min^{-1} by placing the container in a circulator chiller (60:40 vol% ethylene glycol:water mixture). The solvent was removed from the samples by sublimation through lyophylization in a Labconco freeze drier at 7 mtorr (ca., 0.9 Pa) for 48 h. Samples were cooled at a constant rate of $\sim 1^{\circ}$C min^{-1} to produce homogeneous pore sizes throughout the structure. Both tubular and disc shape scaffolds were produced to demonstrate the versatility of the system's applications. Tubular scaffolds (suitable for vascular scaffold applications) were produced by casting the solution in concentric tubes before solidification. Disc shape samples of about 25 mm diameter were also produced and used for characterization.

CHARACTERIZATION

Fourier Transform Infrared Spectroscopy (FTIR)

Samples were characterized with a Nicolet 6700 FT-IR spectrometer (Thermo Electron Corp.) using attenuated total reflectance (ATR) sampling mode and the spectra were processed using OMNIC 7.3 software package. A total of 98 scans with a resolution of 4 cm^{-1} were averaged for each sample.

Particle Size Distribution and Surface Zeta Potential

Particle size distribution was measured for MCC and HMCC samples using NICOMP^{TM} 380 ZLS (Particle Sizing Systems) based on multi-angle dynamic light scattering of the particles in water at 23°C. The wavelength of the laser was 639.0 nm and the water viscosity was set to 0.933 cPoise with refractive index of 1.333, as recommended by the manufacturer for water solutions at 23°C. Three samples were measured with 10 min scanning time and the results were analyzed using CW388 software where the volume weighted distribution was considered for the sample particle size after fitting to a Gaussian curve.

The same instrument was also used to measure the surface zeta potential (ζ-potential) of MCC, HMCC, PLL, MCC/PLL, and HMCC/PLL, dispersed in deionized water at pH 7 with a scattering angle of 14.7° and a scan time of 2 min run^{-1}. Five replicate measurements were performed for each sample. The dielectric constant of 78.5 for water at 23°C, and an electric field strength of 3.5 V/CM were set.

Scaffold Density and Volumetric Porosity

The density and the porosity of the prepared scaffolds were measured by volume displacement, as schematically shown in Fig. 2. A weighed sample of the scaffold was placed in a non-solvent (hexane) that does not swell the polymer. The initial volume of the hexane (V_1) was measured in a narrow test tube (to maximize the liquid displacement), then the sample was immersed in hexane and gently compressed to fill the air-pockets in the structure with the liquid. The sample was left for 5 min to equilibrate and the total volume was measured (V_2). Then the sample was removed and the volume of the remaining hexane was determined (V_3). The volumetric porosity (ε) can be calculated as the volume ratio of the air pockets and the total volume of the scaffold [34]:

$$\varepsilon = \frac{V_1 - V_3}{V_2 - V_3} \tag{1}$$

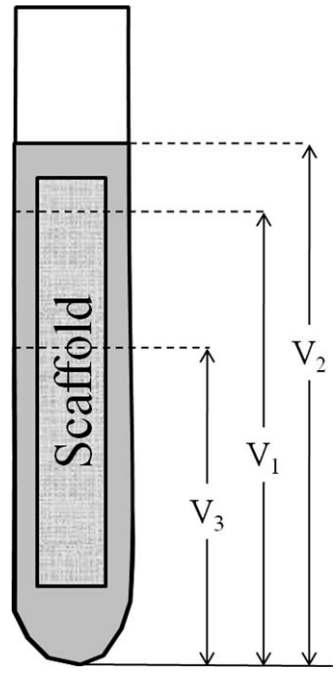

FIG. 2. Measurement of the volumetric porosity and the density of the scaffolds.

The density (ρ) of the scaffold can be calculated as follows:

$$\rho = \frac{m}{V_2 - V_3} \quad (2)$$

where m is the mass of the scaffold sample. The measured porosity is expected to be the minimum porosity of the sample with the assumption that part of the hexane may not penetrate through the scaffold or be removed from the sample before taking its weight.

Swelling

Scaffold samples were first conditioned at an ASTM standard laboratory atmosphere [35] at a temperature of 21°C ± 1°C and a relative humidity of 65% ± 2% for 1 week. Swelling was determined by placing a few drops of deionized water to cover a sample with mass m_1. After 15 min the sample was weighed and the mass recorded as m_2. Percent swelling was calculated based on the water uptake of the sample as:

$$S(\%) = \frac{\mathrm{m}_2 - \mathrm{m}_1}{\mathrm{m}_1} \times 100 \quad (3)$$

Crystallinity

The crystallinity of the samples was measured using Rigaku MiniFlex^{TM} bench-top powder X-ray diffractometer (XRD) equipped with a nickel filtered Cu radiation with a wavelength of $\lambda = 1.541$ Å. The tube output voltage was 30 KV and the current was 15 mA. MCC containing samples were placed in a zero background holder and scanned at $2\theta = 4^\circ$ to 30° at 0.02° increments and a scanning rate of 0.1° min^{-1}. HMCC and their composites were scanned at $2\theta = 5^\circ$ to 60°, to accommodate for the crystallinity peaks of cellulose. To calculate the crystallinity index of a sample, the area under peaks assigned to reflect crystallinity were integrated, then summed and divided by the total area [32].

Surface Morphology

Scanning electron microscopy (SEM) was used to observe the surface morphology of selected samples using a Zeiss EVO 50 scanning electron microscope. The micrographs of MCC and HMCC particles as well as the scaffold samples fabricated at −23°C were characterized with a digital imaging and energy dispersive spectroscopy (EDS) system (Carl Zeiss SMT). The dried samples were mounted on an aluminum stub using a carbon double-sided tape, then sputter-coated with gold using EMS 550X auto sputter coating device (Electron Microscopy Sciences).

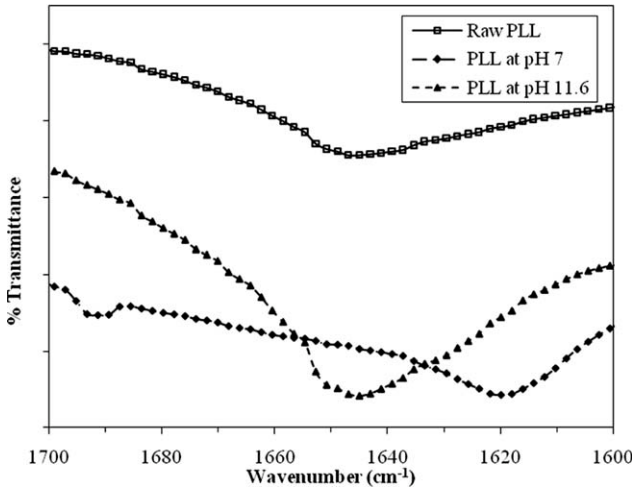

FIG. 3. FTIR spectra for as-received PLL and for PLL dissolved at pH 7 and 11.6.

Statistical Analysis

The descriptive statistics for the resulting data were obtained using a probability value of 95% ($P < 0.05$) to determine the significance. One-way analysis of variance (ANOVA) test was performed to compare groups of data.

RESULTS AND DISCUSSION

Secondary Structure of PLL

PLL was dissolved at pH 7 and 11.6. These pH values were selected because of the physiological pH being about 7.35 at a body temperature of 37.5°C [36] and the pK_a value of PLL being 10.54 [6]. FTIR was used to study the secondary structure of PLL at these pH values where the amide I band is located between 1,610 and 1,690 cm^{-1} [37]. Figure 3 shows the section of the IR spectra that is relevant to this region for as-received PLL and PLL dissolved in pH 7 and 11.6 buffer solutions.

PLL as-received as well as the sample prepared at pH 11.6 showed a band at 1,650 cm^{-1}. In contrast, the spectrum of the sample at pH 7 showed two peaks at about 1,620 and 1,690 cm^{-1}. The band at 1,650 cm^{-1} can be ascribed to the α-helix secondary structure while the peaks at 1,620 and 1,690 cm^{-1} can be assigned to β-platelet sheet secondary structure. The weak peak at 1,690 cm^{-1} indicates anti-parallel conformation of the β-sheet which is usually found in synthetically prepared polypeptides [6].

These results suggested α-helix secondary structure for the as-received PLL which remained in this conformation after dissolved in solutions at pH levels higher than its pK_a value. The polymer assumed β-sheet conformation at neutral pH and in solutions below its pK_a. Besides the pH, the secondary structure is also a strong function of the molecular weight of the PLL [38]. The high molecular

 DOI 10.1002/pc

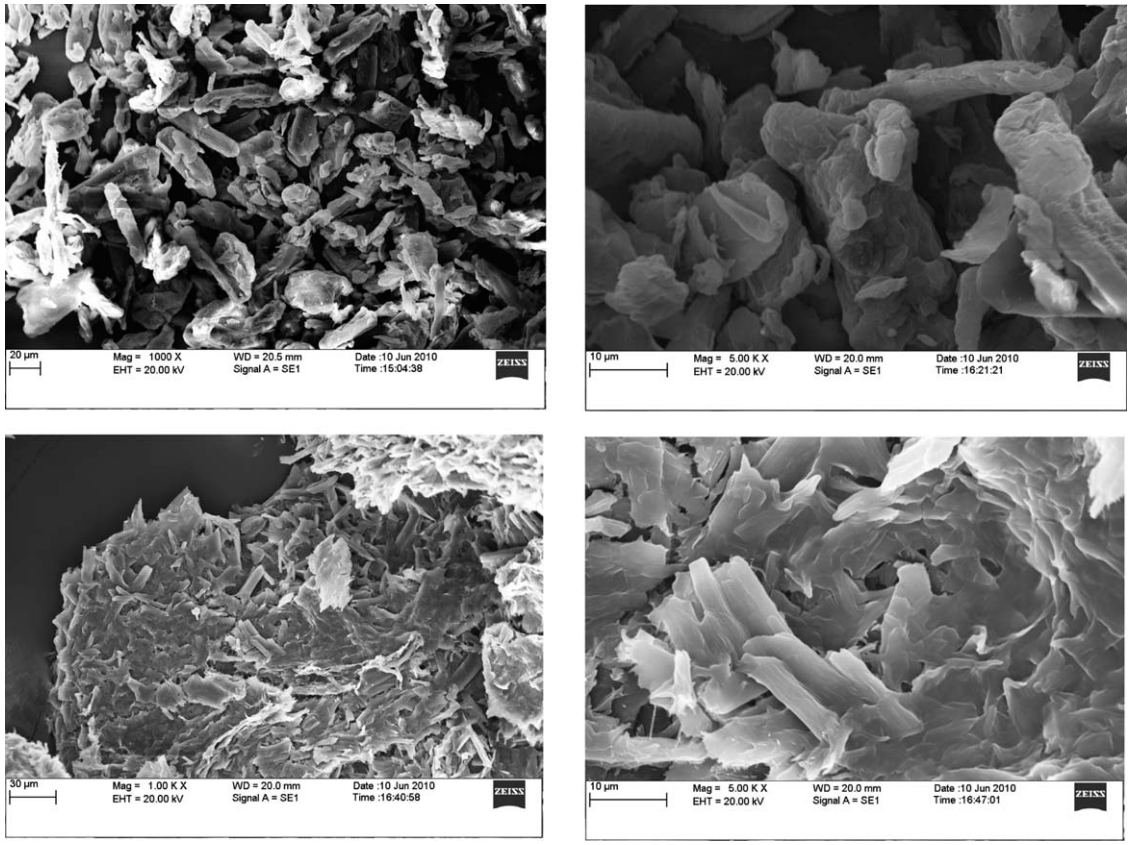

FIG. 4. SEM micrographs for MCC (top) and HMCC (bottom) at different magnifications (a and c at 1 KX and b and d at 5 KX).

weight (150 kD) of PLL used in this study was expected to result in higher transformation from α-helix to β-sheet conformation. The secondary structure of polypeptides is driven by the minimization of the conformational free energy due to hydrogen bonding, the electrostatic interactions, and the van der Waals forces [39]. Therefore, the polymer will be protonated at pH 7 and some cationic charges will develop on the polymer chain that will generate electrostatic repulsive forces. These forces can result in the breaking of the intrachain hydrogen bonds existing in the α-helix conformation and support the transformation to β-sheet structure to minimize the conformational energy of the polypeptide.

Cellulose Hydrolysis

The surface morphology of MCC and HMCC particles is given in Fig. 4. In the case of MCC with an aspect ratio that varied between 2 and 10, a fairly rough surface was observed. After hydrolysis, the particles look smaller and seem to have a flake-like surface.

The X-ray diffractograms of the MCC and HMCC samples are displayed in Fig. 5. The X-ray crystallinity results agreed reasonably well with the reported 50–70% crystallinity ranges for MCC depending on the source of the cellulose [40]. Both hydrolysis methods resulted in about 25% increase in the crystallinity of the particles. The average particle sizes and particle size distributions were determined for the untreated MCC and the hydrolyzed samples and the results are listed in Table 2. Because the size of the particles is given as a distribution, two parameters are usually needed to describe it. One is a measure for the central tendency of the distribution (mean μ), and the second is a measure for the variability

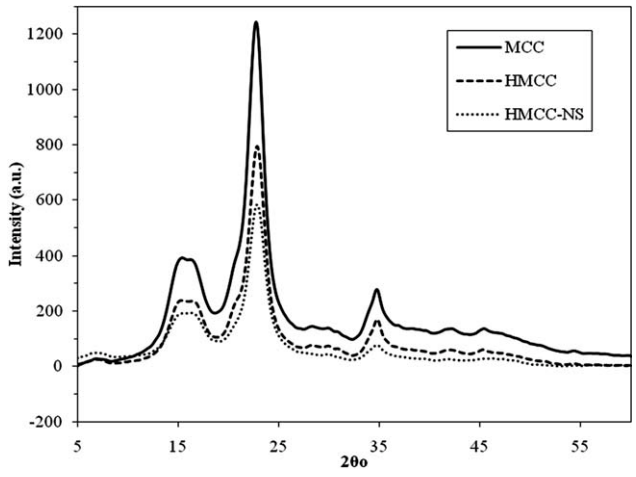

FIG. 5. The XRD diffractograms for MCC, HMCC and HMCC-NS.

TABLE 2. Measured particle size and zeta potential for cellulose particles.

	Particle size			ζ-potential	
	Average size[a] (μm)	Coefficient of variation (C.V.)	χ^2	ζ-potential (mV)	standard deviation (mV)
MCC	12	0.527	1.16	−33.55	1.28
HMCC	0.217	0.561	34.6	−8.13	4.05
HMCC-NS	27.4	0.801	0.336	−7.56	8.24

[a] Volume weighted average size.

(standard of deviation σ). The coefficient of variation is a combined measure parameter for the distribution (CV $= \sigma/\mu \times 100$).

The hydrolysis of MCC affected particle dimensions and surface ζ-potential by decreasing the average size of the particles to the nanometer range (about 200 nm) due to the removal of amorphous regions. When sonication was applied during the hydrolysis process, the resulting particles were relatively well dispersed and fairly small while the average particle size was higher (even higher than the original MCC particles) without sonication. It is possible that without sonication, particle aggregates were formed and resulted in the observed increase in size of the particles.

PLL/Cellulose Composites

The conformation of PLL/MCC composite was determined from the FTIR spectra presented in Fig. 6. All samples had been prepared at pH 7 and formed into porous structures by freeze-drying. Only one band at 1,650 cm^{-1} was observed for all these samples which indicated α-helical structure regardless of pH, composition, or processing method. Obviously, the β-sheet conformation could not

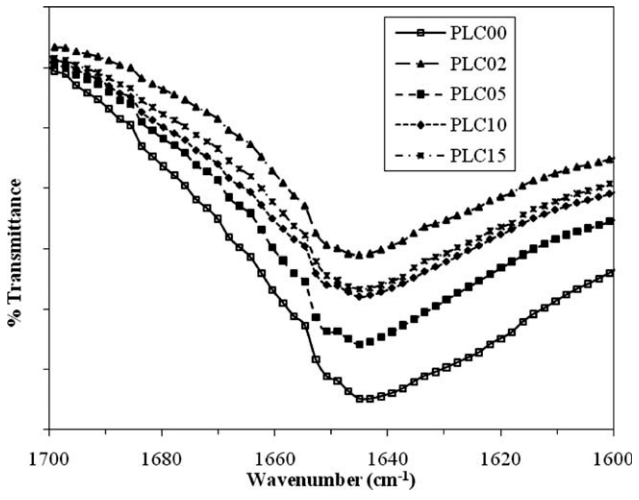

FIG. 6. FTIR spectra for scaffolds with different concentrations of MCC.

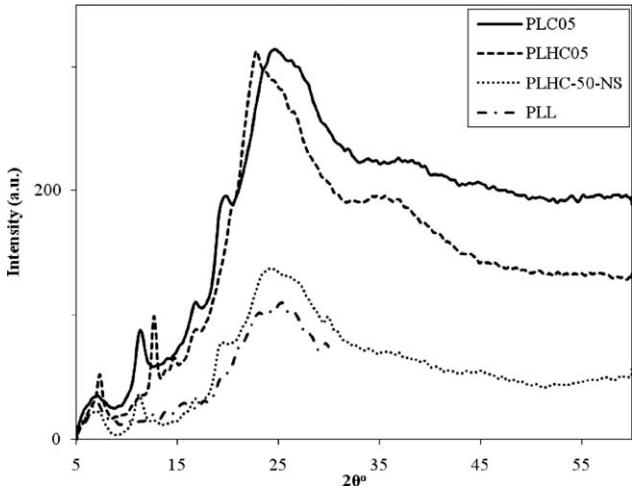

FIG. 7. X-ray diffraction patterns for PLC05, PLHC05, PLHC05-NS, and PLL.

form under any of these conditions. It is possible that the temperature decrease during the freezing step is responsible for the observed conformation and the formation of hydrogen bonding between the polymer chains which would restrict β-sheet formation regardless of the pH value [41].

The ζ-potential for aqueous solution of PLL was found to be 102.34 ± 22.74 mV and 59.98 ± 14.18 mV for a solution with equal amounts of MCC and PLL. These results indicate a decrease in the positive surface potential of PLL with an amount closer to the negative value of MCC ζ-potential. This may imply an electrostatic interaction between the two components of the mixture that can help in a better integration of MCC particles in the PLL matrix.

The as-received PLL sample showed a small peak characteristic for the semi-crystalline PLL [6], as indicated in Fig. 7, and its calculated crystallinity index was ∼24%. X-ray crystallinity results for selected PLL/MCC and PLL/HMCC composite samples are also shown in Fig. 7. The diffractograms for all PLL/MCC composites showed an additional shoulder that had developed after lyophylization. However, the overall crystallinity indices dropped to about 18% on the average which was surprising. The need for incorporating the hydrolyzed MCC into the PLL matrix seemed to be the logical consequence of this finding.

HMCC was incorporated into the PLL in place of MCC at a concentration of 5 wt%. The crystallinity increased from 29% for the PLC05 sample to 33.5% for PLHC05 and to 44% for PLHC05-NS. The X-ray diffraction patterns of these samples are shown in Fig. 7. The crystallinity of the PLL/MCC composites was lower than the crystallinity of the original PLL sample while an increase in the crystallinity was noticed in the samples with HMCC. As expected, the higher crystallinity of HMCC compared to MCC as well as the smaller size of HMCC particles with higher surface area might have

DOI 10.1002/pc

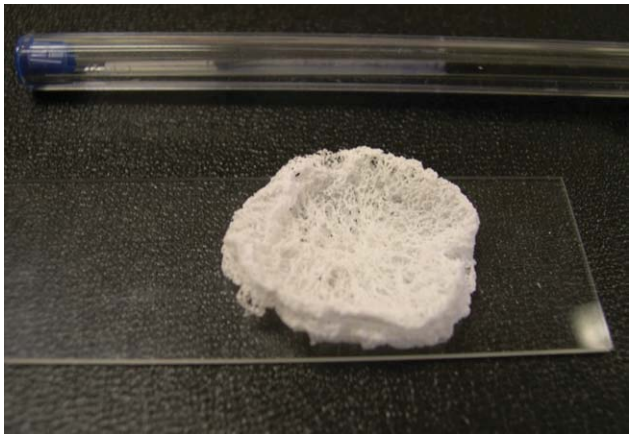

FIG. 8. Disc shaped PLC05 scaffold sample. [Color figure can be viewed in the online issue, which is available at wileyonlinelibrary.com.]

improved the interaction between the cellulose particles and the PLL matrix. The increase in crystallinity was found to correlate with a decrease in the swelling of the composite samples.

Scaffold Fabrication

To produce a scaffold that is sufficiently porous, prepared aqueous solutions for PLL and MCC were pre-frozen at -23°C prior to lyophylization and porous structures were created. A typical example of a scaffold is shown in Fig. 8. The surface morphology of the samples is illustrated in Fig. 9. Without the addition of MCC, the surface appears smoother (Fig. 9a) than in case of samples containing MCC (Fig. 9b, 10% MCC) or HMCC (not shown).

The effect of freezing temperature on the pore size and porosity of the produced scaffolds is driven by the thermodynamics of the polymer solution where phase separation takes place during freezing. The scaffold samples prepared by freezing at -23°C have separate phases of solidified solvent and polymer which were then exposed to a high vacuum (7 mtorr) during lyophylization. Sublimation of the solvent left voids which became a continuous network of pores, a characteristic for the temperature induced phase separation (TIPS) process.

TABLE 3. Volumetric porosity, density, and swelling for scaffolds prepared at different conditions.

	Volumetric porosity (%)	Density (g cm^{-3})	Swelling percentage (%)
PLC00	81.31	0.0945	3428.6
PLC02	92.31	0.0816	1546.3
PLC05	93.83	0.0818	747.0
PLC10	88.57	0.0869	697.5
PLC15	87.34	0.0789	296.6
PLHC05	85.43	0.0748	208.2
PLHC05-NS	86.92	0.0954	102.6

The density and volumetric porosity for scaffolds are listed in Table 3 which shows the impact of processing parameters on the properties of the produced scaffolds. An increase in the volumetric porosity, for example, is expected to result in a decrease of the structure density due to the increase in the void volume. Accordingly, an increase in crystallinity leads to an increase in density of the scaffold structure and a decrease in the swelling of the sample.

Swelling of the scaffold in connection to crystallinity had to be used to express the improved physical stability of the composite samples. As porous structures, the mechanical properties of the scaffolds depend more significantly on the pore size distribution than on the material construction, and cellular solids modeling and analysis techniques [42] are used to study these structures. The irregular thickness and pore size distribution of the scaffolds made it necessary to find alternative methods to express changes in mechanical properties. Swelling seemed to correlate well with the mechanical properties of the material and therefore served in this research as an indirect method to differentiate between the samples' mechanical stability.

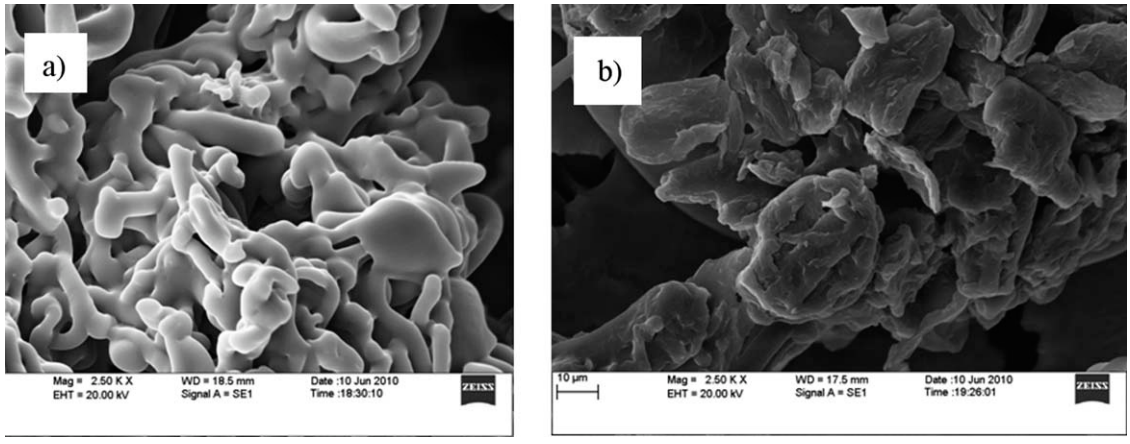

FIG. 9. SEM micrographs of PLC00 (a) and PLC10 (b) samples (2.5 KX).

CONCLUSIONS

The basic hypothesis behind this work was that introducing microcrystalline cellulose (MCC) into poly(L-lysine) (PLL) composite structures may lead to enhanced mechanical properties of PLL. This hypothesis was investigated by studying the conformation of PLL in different pH, modifying the crystallinity of MCC through hydrolysis, including MCC in different proportions, and forming porous structures suitable for scaffold application. Results showed the formation of a composite structure with attractive electrostatic forces between the components and a higher crystallinity if MCC was further hydrolyzed. The secondary structure of PLL was found to be affected by the microenvironmental as well as the processing conditions during freeze-drying. It was observed that the hydrolysis conditions of the MCC particles were crucial in regard to the morphology and the crystallinity of HMCC with a slightly higher crystallization produced at mild hydrolysis condition. The studied samples showed that the inclusion of HMCC particles resulted in an increase of the crystallinity of the PLL composite while MCC particles without further hydrolysis decreased the degree of its crystallinity. Crystallinity and swelling were used as indirect indicators for the mechanical stability of the scaffold.

ACKNOWLEDGMENT

The authors thank Brian Little at the Department of Chemistry and Biochemistry, Auburn University, for assistance with the X-ray diffraction measurements.

REFERENCES

1. P.X. Ma and J.H. Elisseeff, *Scaffolding in Tissue Engineering*, Taylor&Francis, Boca Raton (2005).
2. W.H. Dietmar, S. Thorsten, Z. Iwan, N. Kee Woei, T. Swee Hin, and T. Kim Cheng, *J. Biomed. Mater. Res.*, **55**, 203 (2001).
3. D.W. Hutmacher, *Biomaterials*, **21**, 2529 (2000).
4. L.E. Freed, G. Vunjak-Novakovic, R.J. Biron, D.B. Eagles, D.C. Lesnoy, S.K. Barlow, and R. Langer, *Nat. Biotechnol.*, **12**, 689 (1994).
5. N.J. Benevenga and K.P. Blemings, *J. Nutr.*, **137**, 1610S (2007).
6. R.A. Hule and D.J. Pochan, *J. Polym. Sci. B Polym. Phys.*, **45**, 239 (2007).
7. T. Sawai, S. Yamazaki, Y. Ishigami, Y. Ikariyama, and M. Aizawa, *Macromolecules*, **24**, 5801 (1991).
8. A. Harada, S. Cammas, and K. Kataoka, *Macromolecules*, **29**, 6183 (1996).
9. R. Deutzmann, M. Aumailley, H. Wiedemann, W. Pysny, R. Timpl, and D. Edgar, *Eur. J. Biochem.*, **191**, 513 (1990).
10. M.X. Tang and F.C. Szoka, *Gene Ther.*, **4**, 823 (1997).
11. A. Fissi, O. Pieroni, G. Ruggeri, and F. Ciardelli, *Macromolecules*, **28**, 302 (1995).
12. S.C. De Smedt, J. Demeester, and W.E. Hennink, *Pharma. Res.*, **17**, 113 (2000).
13. P.M. Quinton and C.W. Philpott, *J. Cell. Biol.*, **56**, 787 (1973).
14. S. Senel, G. Bayramoglu, and M.Y. Arica, *Polym. Int.*, **52**, 1169 (2003).
15. J.A. Hubbell, *Curr. Opin. Biotechnol.*, **10**, 123 (1999).
16. G.B. Schneider, A. English, M. Abraham, R. Zaharias, C. Stanford, and J. Keller, *Biomaterials*, **25**, 3023 (2004).
17. K. Akiyoshi, A. Ueminami, S. Kurumada, and Y. Nomura, *Macromolecules*, **33**, 6752 (2000).
18. D.S. Terman, I. Stewart, J. Robinette, R. Carr, and R. Harbeck, *Clin. Exp. Immunol.*, **24**, 231 (1976).
19. G. Orive, S.K. Tam, J.L. Pedraz, and J.-P. Hallé, *Biomaterials*, **27**, 3691 (2006).
20. B.L. Strand, L. Ryan, P.I. Veld, B. Kulseng, A.M. Rokstad, G. Skjak-Braek, and T. Espevik, *Cell Transplant.*, **10**, 263 (2001).
21. J. Varani, D.R. Inman, S.E.G. Fligiel, and W.J. Hillegas, *Cytotechnology*, **13**, 89 (1993).
22. D.C. Alonzo, S.H. Jeffrey, N.G. Nicholas, M.J. Ivette, B.P. Utpal, M.C. Scott, and L. Robert, *J. Biomed. Mater. Res.*, **35**, 513 (1997).
23. U. Hersel, C. Dahmen, and H. Kessler, *Biomaterials*, **24**, 4385 (2003).
24. R.A. Quirk, W.C. Chan, M.C. Davies, S.J.B. Tendler, and K.M. Shakesheff, *Biomaterials*, **22**, 865 (2001).
25. C. Mingyu, G. Kai, L. Jiamou, G. Yandao, Z. Nanming, and Z. Xiufang, *J. Biomater. Appl.*, **19**, 59 (2004).
26. Y. Zhang, J. Li, Y. Shen, M. Wang, and J. Li, *J. Phys. Chem. B*, **108**, 15343 (2004).
27. Y. Ding, J. Liu, X. Jin, H. Lu, G. Shen, and R. Yu, *Analyst*, **133**, 184 (2008).
28. X. Li and R. Pelton, *Ind. Eng. Chem. Res.*, **44**, 7398 (2005).
29. S. Ichiro, N. Yasuhiko, and I. Taisuke, *J. Polym. Sci.*, **57**, 651 (1962).
30. D.J. Mooney, D.F. Baldwin, N.P. Suh, J.P. Vacanti, and R. Langer, *Biomaterials*, **17**, 1417 (1996).
31. S.J. Hollister, *Nat. Mater.*, **4**, 518 (2005).
32. N.E. Marcovich, M.L. Auad, N.E. Bellesi, S.R. Nutt, and M.I. Aranguren, *J. Mater. Res.*, **21**, 870 (2006).
33. X.M. Dong, J.-F. Revol, and D.G. Gray, *Cellulose*, **5**, 19 (1998).
34. J. Guan, K.L. Fujimoto, M.S. Sacks, and W.R. Wagner, *Biomaterials*, **26**, 3961 (2005)..
35. ASTM International, "Standard Practice for Conditioning and Testing Textiles", Standard Designation: D-1776, Vol. 07.01, (2004).
36. J.W. Severinghaus, M. Stupfel, and A.F. Bradley, *J. Appl. Physiol.*, **9**, 189 (1956).
37. H. Susi, S.N. Timasheff, and L. Stevens, *J. Biol. Chem.*, **242**, 5460 (1967).
38. D. Wojciech, M. Takeshi, K. Minoru, and T. Yoshihiro, *Biopolymers*, **73**, 463 (2004).
39. G.D. Rose and R. Wolfenden, *Annu. Rev. Biophys. Biomol. Struct.*, **22**, 381 (1993).
40. A.P. Mathew, K. Oksman, and M. Sain, *J. Appl. Polym. Sci.*, **97**, 2014 (2005).
41. O. Mishima and H.E. Stanley, *Nature*, **396**, 329 (1998).
42. B.A. Harley, J.H. Leung, E.C.C.M. Silva, and L.J. Gibson, *Acta Biomater*, **3**, 463 (2007).

 DOI 10.1002/pc